Topological disclination states for surface acoustic waves

Sheng-Nan Liang,[1] Zhen-Hui Qin,[1] Hua-Yang Chen,[1] Xiao-Chen Sun,[1,2] Jian-Lan Xie,[1] Ze-Guo Chen,[1,2] Si-Yuan Yu,[1,2,3,*] Cheng He,[1,2,3] Ming-Hui Lu,[1,2,3] and Yan-Feng Chen[1,2,3,†]

[1]*National Laboratory of Solid State Microstructures & Department of Materials Science and Engineering, Nanjing University, Nanjing 210093, China*

[2]*Collaborative Innovation Center of Advanced Microstructures, Nanjing University, Nanjing 210093, China*

[3]*Jiangsu Key Laboratory of Artificial Functional Materials, Nanjing University, Nanjing 210093, China*

(Received 12 April 2022; revised 10 October 2022; accepted 8 November 2022; published 28 November 2022)

Surface acoustic waves (SAWs) are widely involved in today's communication and sensing networks. Recent exploration of topological SAWs has provided promising prospects for developing future hybrid SAW devices. In this paper, by designing tight-binding phononic crystals on a semi-infinite substrate, we revealed topological disclination states, i.e., a kind of bound state in topologically condensed matters, for the SAWs. Numerical simulations show that the bound states induced by disclination in the SAW system are more diverse than in previous electromagnetic and mechanical systems. SAW resonances in the disclinations can be efficiently excited by appropriate mechanical stimulation with decent qualities. These states are robust and flexible for design, providing options for future multifunctional and interdisciplinary SAW manipulators, processors, sensors, and other on-chip integrated components.

DOI: 10.1103/PhysRevB.106.174112

I. INTRODUCTION

Surface acoustic waves (SAWs) are mechanical waves traveling along the surface of solid-state materials with elasticity. Thanks to their advantages, e.g., low loss, easy integration, and small footprint, they are widely used in today's wireless communication and sensing industries and are developing rapidly in microfluidics and quantum information, etc. [1]. The discovery of the topological phases of matter is a major achievement in condensed matter physics in this century [2] and has received increasing attention in electromagnetics and mechanics in recent years [3–19]. Among previous discoveries, for example, bosonic topological insulators (TIs) provide antireflection transport of classical waves on their boundaries. Recently, for the SAWs, analogous topological materials have also been proposed and verified experimentally [20–22], offering avenues for advancing acoustic signal processing [23], sensing [24], and (quantum) computing [25].

In crystals, unlike point defects that are easy to eliminate, disclinations are topological defects that are difficult to eliminate by local perturbation [26]. Such defects have a decisive influence on the properties of materials, e.g., strength and plasticity [27,28]. In electronics, these topological defects may induce some interesting phenomena, e.g., melting in two-dimensional (2D) crystals [29–32]. However, due to the difficulty of realizing on-demand molecular disclinations in real crystals, these topological effects remain theoretical in electronics. In the past 2 years, thanks to the ease of fabrication of artificial photonic/phononic crystals (PnCs), topological effects induced by disclinations have been successfully observed in electromagnetic [33–35] and mechanical systems [36,37].

Bound states in the SAWs have long been widely used in sensing and information processing devices (e.g., various resonators and derived filters). As a class of bound states, those topological defects induced by disclination may lead to higher-quality or more functional SAW bound states. In this paper, we propose and investigate the topological disclinations, i.e., a class of topological defects, for the SAWs. By designing tight-binding (TB) PnCs on a semi-infinite substrate, we construct a SAW TI and a further heptagonal topological disclination structure (HTDS). Numerical simulations show that there are SAW resonant states in the HTDS, which we called SAW disclination states. Due to the hybridity of solid-state acoustic waves on a surface, there are still some differences between the disclination states in the SAW system and other systems reported. These states can be efficiently excited by appropriate mechanical stimulation. They are robust to the overall size of the PnC and disorder and have decent qualities even without special optimization. Since these disclination states are not constructed following conventional bulk-edge correspondence, they offer a vision for more compact and robust SAW devices with high performance.

II. MODEL AND THEORY

SAW-PnCs are artificial acoustic microstructures prepared on an infinite half-space [38–41]. This paper uses the finite-element-method-based software COMSOL Multiphysics to simulate our SAW-PnCs. We consider the half-space substrate isotropic and piezoelectric free for simplicity. The Young's modulus E_1, Poisson's ratio v_1, and mass density ρ_1 of the

*yusiyuan@nju.edu.cn
†yfchen@nju.edu.cn

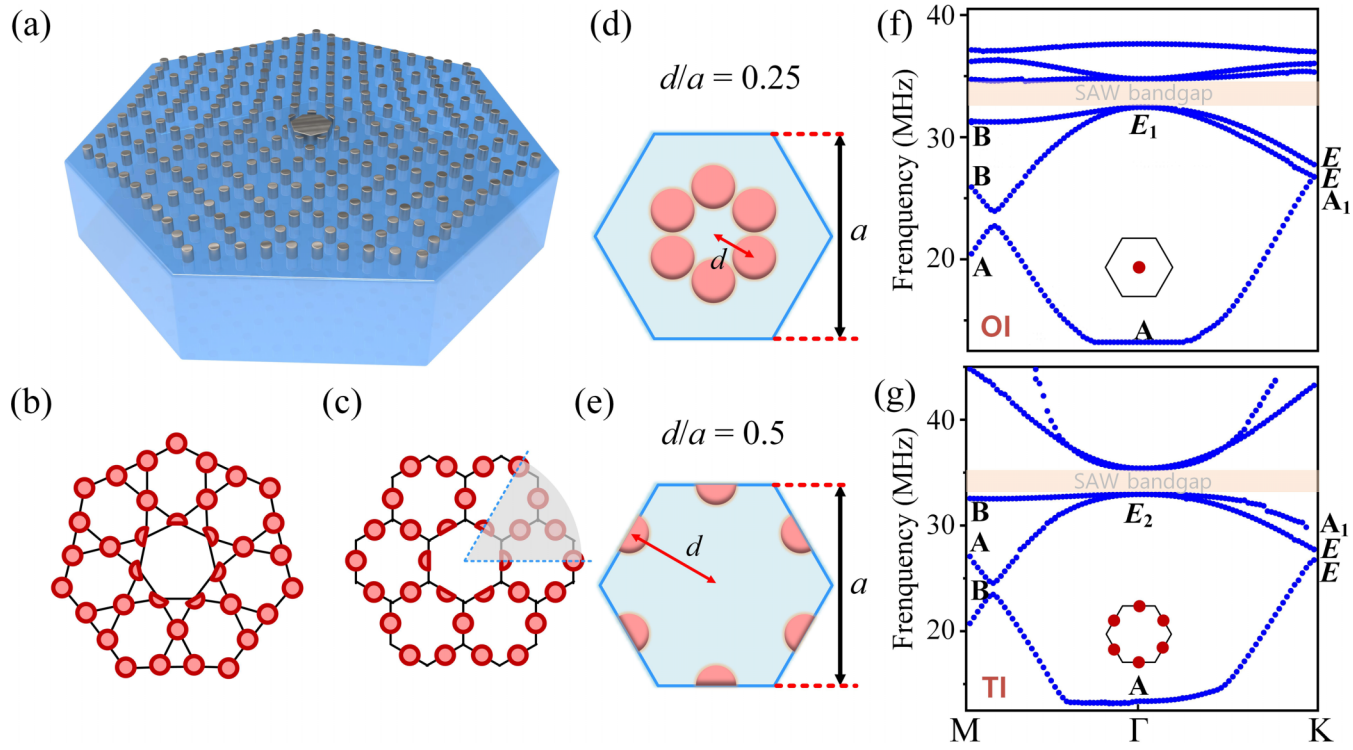

FIG. 1. (a) The heptagonal topological disclination structure (HTDS) for surface acoustic waves (SAWs). (b) Arrangement of atoms (pillars) on the surface of the HTDS. (c) A hexagonal phononic crystal (PnC) in a honeycomb lattice. The gray-marked 60° sector is the basis for our HTDS. Primitive unit cell of our SAW-PnCs: (d) $d/a = 0.25$, and (e) $d/a = 0.5$. Band structures of our SAW-PnC: (f) corresponds to (d), and (g) corresponds to (e).

substrate are 200 GPa, 0.31, and 4700 kg/cm^3, respectively. The artificial microstructures on the substrate surface are micropillars. Their Young's modulus E_2, Poisson's ratio v_2, and mass density ρ_2 are 219 GPa, 0.31, and 8900 kg/cm^3, respectively. All micropillars have the same radius r and height h (equal to $0.2a$ and $0.5a$, respectively) and are acoustically coupled adjacently through the substrate, forming our SAW-PnC.

Figure 1(a) shows a schematic of our HTDS, the basis for SAW topological disclination states (TDSs). The arrangement of atoms (i.e., micropillars) on its surface is shown in Fig. 1(b). The origin of the structure is a hexagonal PnC in a honeycomb lattice, as shown in Fig. 1(c). We take out the $\frac{1}{6}$ area of the PnC (that is, a 60° sector), make seven copies of it, and connect the copies into a heptagonal area with slight compression, constituting the HTDS.

According to previous literature [33,34], crystal disclinations based on ordinary insulators (OIs) often do not have TDSs, so our basic requirement is to construct a SAW-TI. As shown in the figure, each unit cell in this PnC has six pillars, and we set the lattice constant $a = 50$ μm (just for demonstration since the whole PnC is scalable). The physical parameters given in this paper are experimentally achievable. Such 2D pillar-type PnCs on the surface of semi-infinite substrates have been experimentally confirmed [42–44], in which both the 2D/one-dimensional (1D) propagating states and the 1D/zero-dimensional (0D) localized states have been experimentally well realized. Theoretically, in acoustics/mechanics, periodic columnar arrays on the surface of an elastic substrate (i.e., our PnC) can theoretically be equivalent to substrates with periodically attached spring-mass resonators [45]. Such an acoustic model can be further processed by TB theory [46,47] to derive many kinds of artificial microstructured materials, e.g., acoustic graphene [48]. Also, under the TB theory, the honeycomb PnC can be equated to a honeycomb Su-Schrieffer-Heeger (SSH) model [49,50]. Like the 1D [46] and 2D SSH models [47], the topological phase transition from an OI to a TI (and vice versa) can be realized by adjusting the value of its intercell and intracell coupling. In our SAW-PnC, the coupling regulation can be achieved by changing the distance of every micropillar to the center of the primitive unit cell, as shown in Figs. 1(d) and 1(e). When the micropillars in the unit cell are close to the center [e.g., $d/a = 0.25$ in Fig. 1(d)], the intercell coupling of the TB model corresponding to this PnC is smaller than the intracell coupling; a SAW-OI can be achieved. When the pillars in the unit cell are far from the center [e.g., $d/a = 0.5$ in Fig. 1(e)], the intercell coupling is larger than the intracell coupling; a SAW-TI can be achieved. The band structures of the SAW-OI, SAW-TI, and corresponding SAW conduction modes are shown in Figs. 1(f) and 1(g), respectively.

SAW-TI and SAW-OI have different responses to the disclination structure, which can be defined by the fractional disclination charge extracted [51,52]. Meanwhile, the fractional disclination charge can be deduced from the topological index, where the topological index is given by

$$\chi = (\chi_M, \chi_K), \tag{1}$$

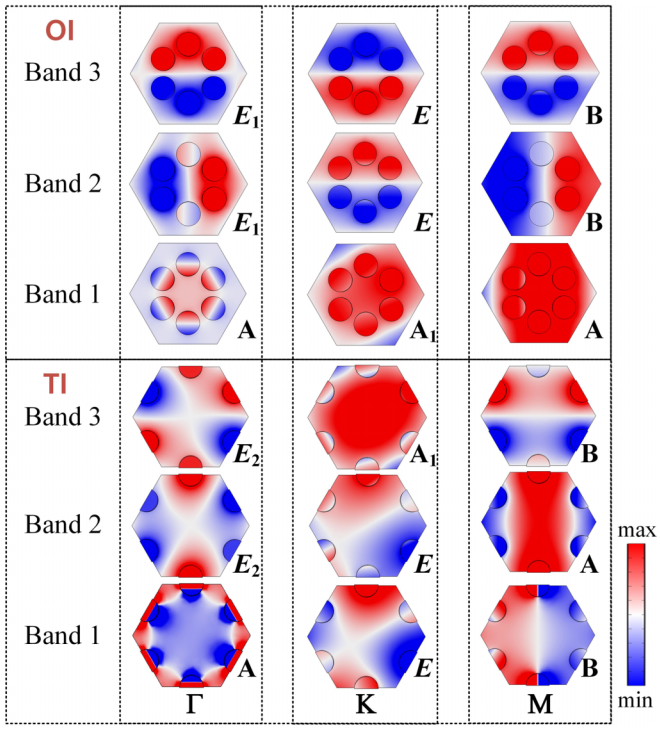

FIG. 2. Out-of plane displacement fields of the eigenmodes at the high-symmetry points (HSPs) for the trivial ($d/a = 0.25$) and topological ($d/a = 0.5$) surface acoustic wave (SAW) phononic crystals (PnCs). The eigenmodes are also labeled in the figure using the irreducible representations of the little group at the HSPs, which corresponds to the three occupied bands in Figs. 1(f) and 1(g), respectively.

where $\chi_M = [M_1^{(2)}]$ and $\chi_K = [K_1^{(3)}]$ are the symmetry indicators of high-symmetry points (HSPs) M and K, respectively. In general, if $\chi \neq (0,\ 0)$, the band topology is nontrivial. The symmetry indicator is determined by the eigenmode of the HSP, which satisfies

$$\left[\Pi_p^{(n)}\right] = \#\Pi_p^{(n)} - \#\Gamma_p^{(n)}, \tag{2}$$

where $\#\Pi_p^{(n)}$ is the number of occupied bands below the bandgap at HSP Π with the rotation eigenvalue $\Pi_p^{(n)} = \exp[2\pi i(p-1)n]$, while p is an integer in the range of 1 to n. In the C_6 structure, the HSP $\Pi^{(n)}$ stands for $\Pi^{(6)} = \Gamma$; $\Pi^{(3)} = \Gamma$, K, and K'; and $\Pi^{(2)} = \Gamma$, M, M', and M''.

According to previous research [33], for the SAW-PnCs, we apply the symmetry indicators of the eigenmodes at the HSPs to obtain the topological index. As shown in Fig. 2, we present the displacement field (Z) profiles at the HSPs for the trivial ($d/a = 0.25$) and topological ($d/a = 0.5$) SAW-PnCs. One can obtain all the symmetry indicators at the HSPs from the displacement field profiles, which gives the following results for all the HSPs and all three bands below the bandgap. For the C_6-symmetric TI and OI in this paper, $M_1^{(2)}$ and $K_1^{(3)}$ of OI are both 0, while $M_1^{(2)}$ and $K_1^{(3)}$ of TI are -2 and 0, respectively. Finally, the fractional disclination charge Q_{dis} can be deduced from the topological index, that is,

$$Q_{\text{dis}} = \frac{\Omega}{2\pi}\left[\frac{3}{2}M_1^{(2)} + 2K_1^{(3)}\right] \text{mod} 1, \tag{3}$$

where Ω is the Frank angle, i.e., the angle of the copying sector. In this paper, $\Omega = \frac{\pi}{3}$. According to the topological indices of TI and OI, their Q_{dis} are $-\frac{1}{2}$ and 0, respectively. Therefore, the HTDS constructed by SAW-TI has nonzero Q_{dis}, indicating it could support the TDSs.

It should be noted that the fractional disclination charge of the system is consistent during the process from TI to the phase transition point (i.e., the semimetal), as shown in the previous research [33].

To simplify our HTDS, a limit case of a SAW-TI is taken in this paper, i.e., $d/a = 0.5$. At this time, the edge region of the primitive unit cell is shared not only by the Wannier center [the insert in Fig. 1(g)] but also by the micropillars [33]. In the above analyses, we constructed a SAW-TI. Now, as mentioned before, we use a 60° sector of the SAW-TI, make seven copies of it, and connect all the copies into a heptagonal area with slight compression, constituting the HTDS for SAWs.

III. RESULTS AND DISCUSSIONS

To verify there exist SAW TDSs in the HTDS, we first model an HTDS sample with 105 unit cells and calculate all its SAW eigenstates within the bandgap of the TI and its nearby bulk. As shown in Fig. 3, like in previous studies, the realization of disclination states can be induced by constructing HTDS using TI, and the number of these disclination states is related to the rotational symmetry of the HTDS, which is also consistent with previous studies. However, different from previous studies, some SAW disclination states are no longer located in the bandgap, as shown by the purple pentagram in Fig. 3. Thus, we classify the disclination states in the SAW system into (1) TDSs located in the bandgap and (2) ordinary disclination states (ODSs) located in the bulk band. In addition to the above seven disclination states, we also found some bounded states (BSs) around the disclination in our SAW system. All these SAW resonant states exhibit strong bound properties, i.e., the SAWs are collected in the middle region of HTDS. Different types of SAW resonant states have different bound properties, but all of them show a star-shaped pattern that spreads out from the center of the HTDS. Based on the symmetry of three kinds of SAW resonant states, we grouped these states into seven categories and labeled these states from φ_{I} to φ_{VII}. The BSs, i.e., φ_{I}, φ_{II}, and φ_{III}, confine the SAWs to the third circle of micropillars from the HTDS center, while φ_{I} exhibits a more heptagonal pattern but φ_{III} presents a more circular pattern. The TDSs, i.e., φ_{IV}, φ_{V}, and φ_{VI}, confine the SAWs near the center of the HTDS, like previous studies in electromagnetic systems [33,34]. On the contrary, the ODSs labeled by φ_{VII} confine most SAWs near the center of the HTDS but with some leakage into the bulk modes.

These SAW resonant states achieved by the SAW HTDS are structurally robust. If we increase the number of unit cells of the HTDS from 105 to 252, there are still four BSs, five TDSs, and two ODSs calculated by the same method, and their SAW patterns and eigenfrequencies remain unchanged. The SAW field distribution and theoretical quality factor (Q) of SAW resonant states are shown in Fig. 4. It can be seen that the TDSs have higher Q than the ODSs. This is reasonable since the ODSs are leaky modes. It is worth noting that all BSs

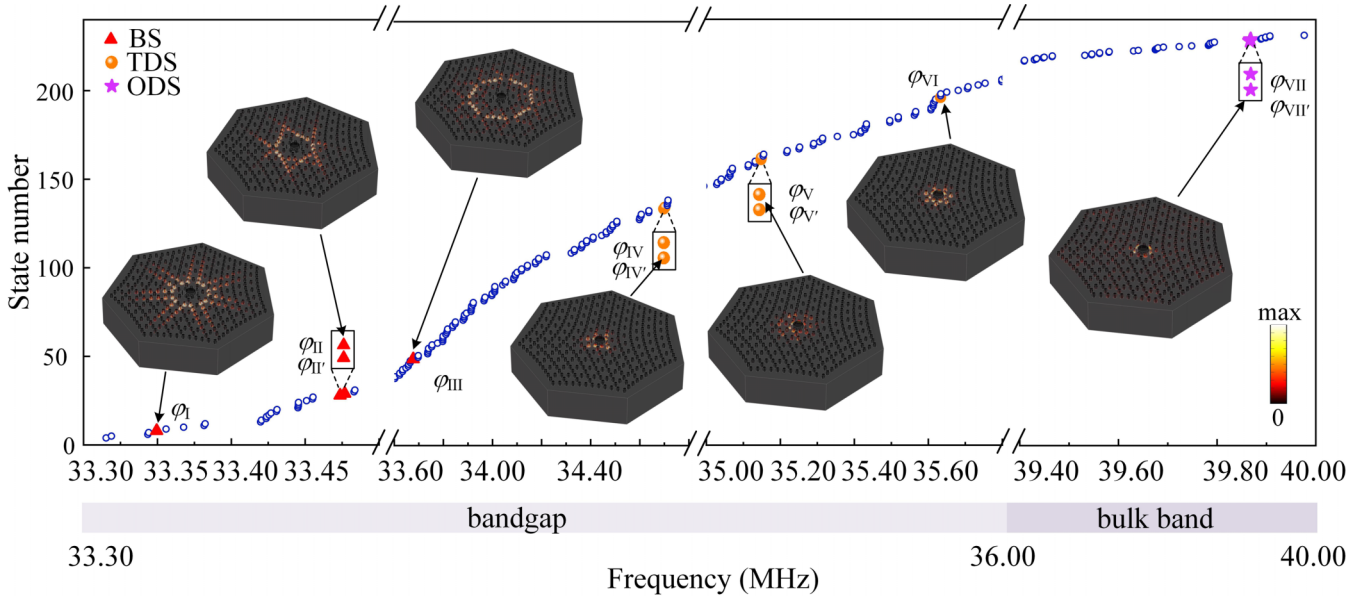

FIG. 3. Numbers of the surface acoustic wave (SAW) eigenstates in our heptagonal topological disclination structure (HTDS). The insets demonstrate SAW energy fields of three different kinds of SAW resonant states, where the red triangles, orange spheres, and purple pentagram represent the bounded states (BSs), topological disclination states (TDSs), and ordinary disclination state (ODS), respectively. The bulk band and bandgap are distinguished by different colors below the figure, where dark gray represents the bulk band and light gray represents the bandgap.

induced by the disclinations have relatively higher Q (over an order of magnitude), although their mode volumes are larger.

To verify the robustness of the SAW resonant states, we calculate the SAW resonant eigenstates in a HTDS with disorder, as shown in Fig. 5. The disorder is created by randomly shifting several micropillars in the substrate surface, yielding a partially amorphous lattice. Simulated energy distribution shows that, even in the presence of this disorder, the TDSs and BSs remain unchanged but the ODSs disappear (or at least deviate greatly from the original frequency).

All these SAW topological resonant states can be efficiently excited by appropriate mechanical stimulations, i.e., sources. To avoid losing generality, we take the HTDS consisting of 252 unit cells as an example and excite all these topological resonant states by setting different point stimulations. Under their excitations, SAW field distributions and calculated Q values of all topological resonant states are shown in Fig. 6.

Figure 6(a) shows that, for the TDSs φ_{IV}, $\varphi_{\mathrm{IV}'}$, φ_{V}, $\varphi_{\mathrm{V}'}$, and φ_{VI}, which all confine the SAWs near the center of the

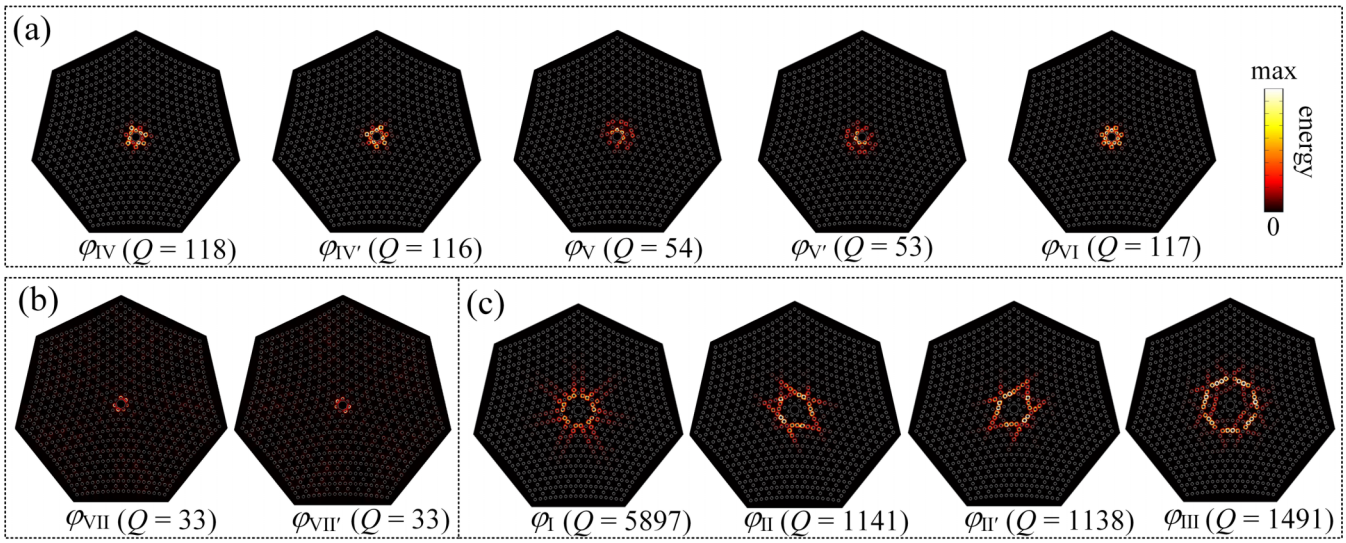

FIG. 4. All calculated surface acoustic wave (SAW) resonant eigenstates in a larger heptagonal topological disclination structure (HTDS) made of 252 unit cells and calculated quality factors (Q) of each state. (a) Topological disclination states (TDSs), (b) ordinary disclination states (ODSs), and (c) bounded states (BSs).

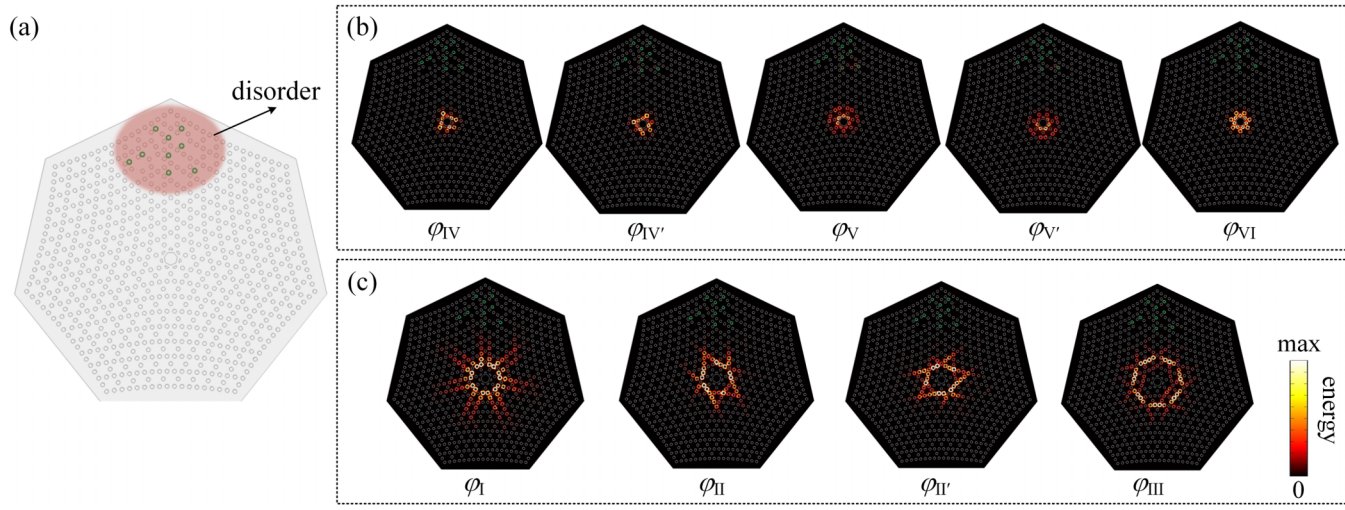

FIG. 5. All calculated topological resonant eigenstates in a larger heptagonal topological disclination structure (HTDS) made of 252 unit cells and with an disorder. (a) HTDS with a disorder yielding a partially amorphous lattice, (b) topological disclination states (TDSs), and (c) bounded states (BSs).

HTDS, only one point source is needed for their excitation. Because these states have different spatial symmetries, the positions and phases of their corresponding sources are also different. Like the five TDSs, the four discovered BSs can also be excited, and their Q are also in line with expectations. Specifically, the BS φ_{I} needs to be excited by two (pairs of) point sources with antisymmetric modes (i.e., the phase difference is 180°), and the positions of these two point sources are located at the two vertices of the heptagonal field excited by the state. The BSs φ_{II} and $\varphi_{II'}$ can be excited by only one point source, located at the farthest corner of the field excited by the states. The BS φ_{III} needs to be excited by two (pairs of) point sources with antisymmetric modes, both located at the two vertices of the heptagonal field excited by the state (same as φ_{I}).

Under excitations, we calculated the Q values for different SAW TDSs by the 3 dB bandwidth of their energy spectra. Their Q values are roughly the same as those obtained by

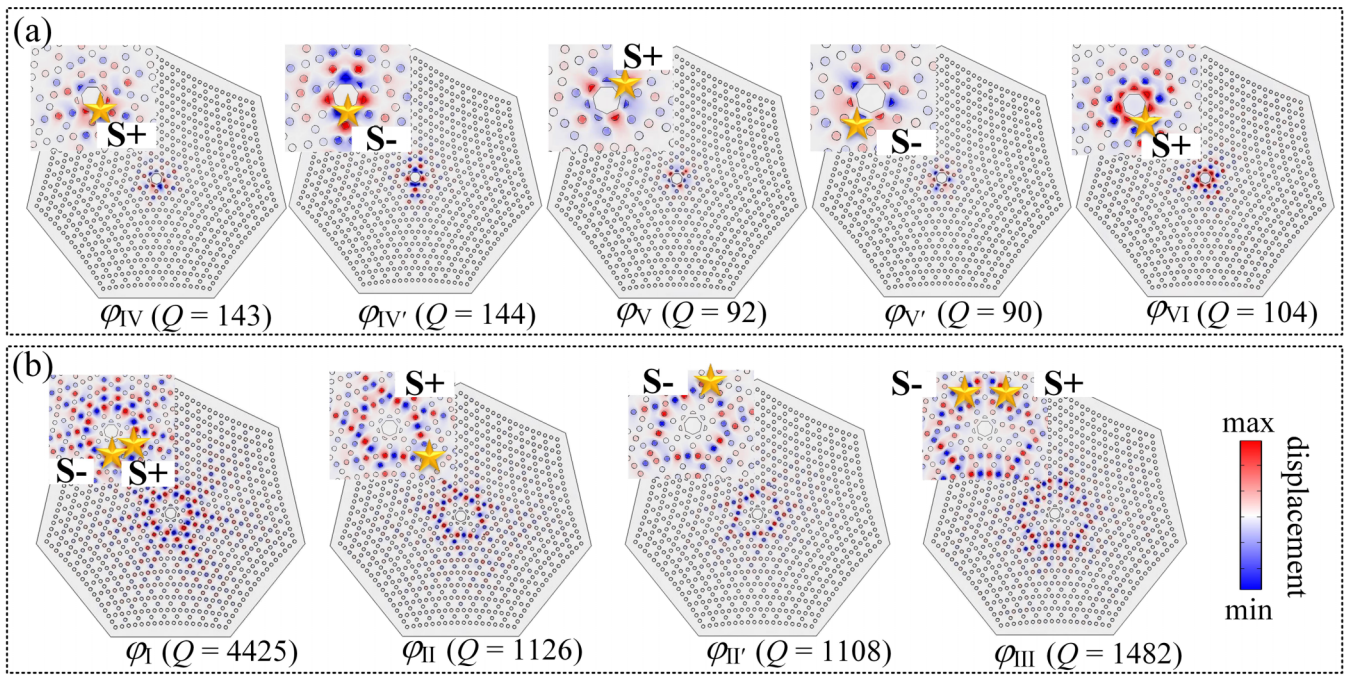

FIG. 6. Exicated surface acoustic wave (SAW) topological resonant states in the heptagonal topological disclination structure (HTDS) made of 252 unit cells and measured quality factors (Q) of each excited state. (a) Topological disclination states (TDSs) and (b) bounded states (BSs).

eigenstate calculation in Fig. 4, ranging from tens to thousands. Since we did not perform any design optimization for all of these topological resonant states, we believe that topological resonant states with higher quality factors (e.g., $Q > 10\,000$) are possible by design. This kind of SAW BSs with topologically protected robustness may provide a case study of collective modes in classical wave systems. For practical applications, they may also inspire ideas for developing interdisciplinary and multifunctional SAW manipulators, sensors, and information processors.

IV. CONCLUSION

In this paper, we investigate TDSs, i.e., a kind of collective mode in topologically condensed matter, for the SAWs, via constructing an HDTS using a SAW-TI. In contrast to previous studies in electromagnetic and mechanical systems, the hybridity of solid-state acoustic waves on a surface allows us to realize more diverse topological resonant states induced by the disclination. Through simple structural transformation, these topological resonant states can localize the SAWs well around the center of the HTDS. They can be excited selectively and efficiently with decent qualities exceeding 10^4 (or even higher). Our proposed PnCs can be obtained by fabricating metal (e.g., Ni, Cu, Au) pillar arrays on the surface of the piezoelectric substrate (e.g., lithium niobate) [42–44] or directly etched on nonpiezoelectric (e.g., silicon) substrate [53]. Meanwhile, these SAW resonant states can be excited by fabricating additional electrodes, mechanical excitation, or using laser ultrasound [54]. For the observations of the excited SAW disclination states, a conventional vibrometer using laser interferometry is sufficient [55]. Testing techniques such as the use of microwave near fields [56] can also be employed. The realization of these SAW topological states offers a methodology for SAW manipulations and provides ideas for high-performance SAW sensing, information processing (such as filters), energy harvesting, or future acoustic-based quantum computing, etc.

ACKNOWLEDGMENTS

This paper was jointly supported by the National Key R&D Program of China (No. 2022YFA1404404 and No. 2021YFB3801801) and the National Natural Science Foundation of China (No. 11890702, No. 92163133, No. 52022038, and No. 52103341). We also acknowledge the support of Fundamental Research Funds for Central Universities.

[1] P. Delsing, A. N. Cleland, M. J. A. Schuetz, J. Knörzer, G. Giedke, J. I. Cirac, K. Srinivasan, M. Wu, K. C. Balram, C. Bäuerle *et al.*, J. Phys. D: Appl. Phys. **52**, 353001 (2019).
[2] A. Bansil, H. Lin, and T. Das, Rev. Mod. Phys. **88**, 021004 (2016).
[3] F. D. M. Haldane and S. Raghu, Phys. Rev. Lett. **100**, 013904 (2008).
[4] Z. Wang, Y. Chong, J. D. Joannopoulos, and M. Soljacic, Nature (London) **461**, 772 (2009).
[5] L.-H. Wu and X. Hu, Phys. Rev. Lett. **114**, 223901 (2015).
[6] Y. Yang, Y. F. Xu, T. Xu, H.-X. Wang, J.-H. Jiang, X. Hu, and Z. H. Hang, Phys. Rev. Lett. **120**, 217401 (2018).
[7] J.-W. Dong, X.-D. Chen, H. Zhu, Y. Wang, and X. Zhang, Nat. Mater. **16**, 298 (2017).
[8] B.-Y. Xie, H.-F. Wang, H.-X. Wang, X.-Y. Zhu, J.-H. Jiang, M.-H. Lu, and Y.-F. Chen, Phys. Rev. B **98**, 205147 (2018).
[9] Z. Yang, F. Gao, X. Shi, X. Lin, Z. Gao, Y. Chong, and B. Zhang, Phys. Rev. Lett. **114**, 114301 (2015).
[10] C. He, X. Ni, H. Ge, X.-C. Sun, Y.-B. Chen, M.-H. Lu, X.-P. Liu, and Y.-F. Chen, Nat. Phys. **12**, 1124 (2016).
[11] J. Lu, C. Qiu, L. Ye, X. Fan, M. Ke, F. Zhang, and Z. Liu, Nat. Phys. **13**, 369 (2017).
[12] M. Serra-Garcia, V. Peri, R. Süsstrunk, O. R. Bilal, T. Larsen, L. G. Villanueva, and S. D. Huber, Nature (London) **555**, 342 (2018).
[13] A. B. Khanikaev and G. Shvets, Nat. Photon. **11**, 763 (2017).
[14] X. Zhang, M. Xiao, Y. Cheng, M.-H. Lu, and J. Christensen, Commun. Phys. **1**, 97 (2018).
[15] T. Ozawa, H. M. Price, A. Amo, N. Goldman, M. Hafezi, L. Lu, M. C. Rechtsman, D. Schuster, J. Simon, O. Zilberberg, and I. Carusotto, Rev. Mod. Phys. **91**, 015006 (2019).
[16] M. I. Shalaev, W. Walasik, A. Tsukernik, Y. Xu, and N. M. Litchinitser, Nat. Nanotechol. **14**, 31 (2019).
[17] G. Ma, M. Xiao, and C. T. Chan, Nat. Rev. Phys. **1**, 281 (2019).
[18] M. Kim, Z. Jacob, and J. Rho, Light-Sci. Appl. **9**, 130 (2020).
[19] B. Xie, H.-X. Wang, X. Zhang, P. Zhan, J.-H. Jiang, M. Lu, and Y. Chen, Nat. Rev. Phys. **3**, 520 (2021).
[20] T. Inoue and S. Murakami, Phys. Rev. B **99**, 195443 (2019).
[21] Y.-H. Wang, Z.-W. Zhang, Y. Cheng, and X.-J. Liu, Acta Phys. Sin. **68**, 227805 (2019).
[22] Z. Wang, F.-K. Liu, S.-Y. Yu, S.-L. Yan, M.-H. Lu, Y. Jing, and Y.-F. Chen, J. Appl. Phys. **125**, 044502 (2019).
[23] C. Campbell, *Surface Acoustic Wave Devices and Their Signal Processing Applications* (Academic Press, Inc., San Diego, 1989).
[24] K. Länge, B. E. Rapp, and M. Rapp, Anal. Bioanal. Chem. **391**, 1509 (2008).
[25] F. VanGessel, J. Peng, and P. W. Chung, J. Mater. Sci. **53**, 5641 (2018).
[26] N. D. Mermin, Rev. Mod. Phys. **51**, 591 (1979).
[27] M. T. Lusk and L. D. Carr, Phys. Rev. Lett. **100**, 175503 (2008).
[28] Y. Wei, J. Wu, H. Yin, X. Shi, R. Yang, and M. Dresselhaus, Nat. Mater. **11**, 759 (2012).
[29] D. R. Nelson and J. M. Kosterlitz, Phys. Rev. Lett. **39**, 1201 (1977).
[30] B. I. Halperin and D. R. Nelson, Phys. Rev. Lett. **41**, 121 (1978).
[31] D. R. Nelson and B. I. Halperin, Phys. Rev. B **19**, 2457 (1979).
[32] J. M. Kosterlitz, Rev. Mod. Phys. **89**, 040501 (2017).
[33] Y. Liu, S. Leung, F.-F. Li, Z.-K. Lin, X. Tao, Y. Poo, and J.-H. Jiang, Nature (London) **589**, 381 (2021).
[34] S. Wu, B. Jiang, Y. Liu, and J.-H. Jiang, Photon. Res. **9**, 668 (2021).

[35] Q. Wang, H. Xue, B. Zhang, and Y. D. Chong, Phys. Rev. Lett. **124**, 243602 (2020).
[36] B. Xia, Z. Jiang, L. Tong, S. Zheng, and X. Man, Acta Mech. Sin. **38**, 521459 (2022).
[37] Y. Deng, W. A. Benalcazar, Z.-G. Chen, M. Oudich, G. Ma, and Y. Jing, Phys. Rev. Lett. **128**, 174301 (2022).
[38] B. J. Ash, S. R. Worsfold, P. Vukusic, and G. R. Nash, Nat. Commun. **8**, 174 (2017).
[39] D. Yudistira, A. Boes, B. Djafari-Rouhani, Y. Pennec, L. Y. Yeo, A. Mitchell, and J. R. Friend, Phys. Rev. Lett. **113**, 215503 (2014).
[40] S.-Y. Yu, X.-C. Sun, X. Ni, Q. Wang, X.-J. Yan, C. He, X.-P. Liu, L. Feng, M.-H. Lu, and Y.-F. Chen, Nat. Mater. **15**, 1243 (2016).
[41] L. Shao, W. Mao, S. Maity, N. Sinclair, Y. Hu, L. Yang, and M. Lončar, Nat. Electron. **3**, 267 (2020).
[42] Y. Achaoui, A. Khelif, S. Benchabane, L. Robert, and V. Laude, Phys. Rev. B **83**, 104201 (2011).
[43] Z.-D. Zhang, S.-Y. Yu, H. Ge, J.-Q. Wang, H.-F. Wang, K.-F. Liu, T. Wu, C. He, M.-H. Lu, and Y.-F. Chen, Phys. Rev. Appl. **16**, 044008 (2021).
[44] J.-Q. Wang, Z.-D. Zhang, S.-Y. Yu, H. Ge, K.-F. Liu, T. Wu, X.-C. Sun, L. Liu, H.-Y. Chen, C. He *et al.*, Nat. Commun. **13**, 1324 (2022).
[45] Y. Xiao, J. Wen, and X. Wen, J. Phys. D: Appl. Phys. **45**, 195401 (2012).
[46] J. K. Asbóth, L. Oroszlány, and A. Pályi, *A Short Course on Topological Insulators* (Springer, Cham, 2016).
[47] F. Liu and K. Wakabayashi, Phys. Rev. Lett. **118**, 076803 (2017).
[48] D. Torrent, D. Mayou, and J. Sánchez-Dehesa, Phys. Rev. B **87**, 115143 (2013).
[49] F. Liu, H.-Y. Deng, and K. Wakabayashi, Phys. Rev. Lett. **122**, 086804 (2019).
[50] Y. Yang, Z. Jia, Y. Wu, R.-C. Xiao, Z. H. Hang, H. Jiang, and X. C. Xie, Sci. Bull. **65**, 531 (2020).
[51] T. Li, P. Zhu, W. A. Benalcazar, and T. L. Hughes, Phys. Rev. B **101**, 115115 (2020).
[52] W. A. Benalcazar, T. Li, and T. L. Hughes, Phys. Rev. B **99**, 245151 (2019).
[53] M. Yan, J. Lu, F. Li, W. Deng, X. Huang, J. Ma, and Z. Liu, Nat. Mater. **17**, 993 (2018).
[54] K. J. Harke, N. Calta, J. Tringe, and D. Stobbe, Sci. Rep. **12**, 3309 (2022).
[55] K. Yao and F. E. H. Tay, IEEE Trans. Ultrason. Ferroelectr. Freq. Control **50**, 113 (2003).
[56] D. Lee, Q. Liu, L. Zheng, X. Ma, H. Li, M. Li, and K. Lai, Phys. Rev. Appl. **16**, 034047 (2021).